ACS APPLIED NANO MATERIALS

www.acsanm.org Article

Interfacial Oxidation of Metals on Graphene

Zhien Wang, Haozhe Wang, Roman Caudillo, Jiangtao Wang, Zhenjing Liu, Alexandre Foucher, Ji-Hoon Park, Meng-Chi Chen, Ang-yu Lu, Peng Wu, Jiadi Zhu, Xudong Zheng, Tymofii S. Pieshkov, Steven A. Vitale, Yimo Han, Frances M. Ross, Iwnetim I. Abate, and Jing Kong*

Cite This: ACS Appl. Nano Mater. 2024, 7, 24537−24546 Read Online

ACCESS Metrics & More | Article Recommendations | Supporting Information

Downloaded via RICE UNIV on March 17, 2025 at 19:43:56 (UTC).
See https://pubs.acs.org/sharingguidelines for options on how to legitimately share published articles.

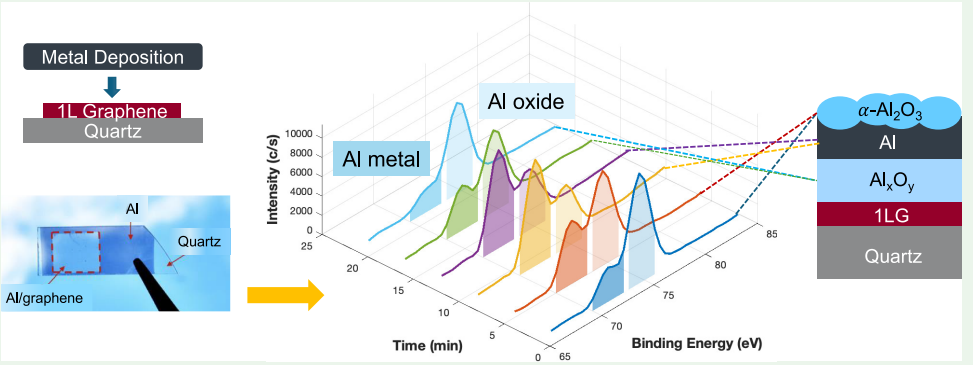

ABSTRACT: In this work, we report the graphene-promoted formation of an interfacial oxide layer when certain metals are deposited on graphene. We probe interfacial oxide formation through the observation that several metals, when 10−12 nm in thickness and deposited on graphene on a transparent substrate, show a change in optical contrast compared to that in areas where the metal directly contacts the substrate. Aluminum shows this effect, while platinum and nickel do not exhibit such a pronounced optical contrast change. To understand this phenomenon, we characterize the Al-graphene, Ti-graphene, and Ni-graphene interfaces using techniques including X-ray photoelectron spectroscopy depth profiling, X-ray reflectivity, and Raman spectroscopy. These techniques show the presence of oxide at the buried metal−graphene interface for the cases of aluminum and titanium deposition, and we discuss how this explains the change in optical contrast. We show that this process is sensitive to the background vacuum level during deposition. In the case of nickel, we did not observe the presence of an oxide. Building upon these findings, we propose structures for Al-graphene, Ti-graphene, and Ni-graphene interfaces. We propose a model based on the metal work function and interaction with graphene that can guide the metals for which interfacial oxidation is to be expected, and we discuss the role of the deposition conditions in controlling the extent of oxide formation. These observations provide important implications for various devices using graphene as either the channel or the contact. Depending on whether a metal−graphene interfacial oxide is desirable and its functionality, these findings will afford guidance for their fabrications in the future.

KEYWORDS: *metal−graphene interface, evaporation, interfacial oxidation, chemical vapor deposition, work function*

INTRODUCTION

Since the successful isolation of graphene,[1−3] two-dimensional materials have expanded to more than 150 categories distinguished by unique electronic structures and properties.[4] Graphene, in particular, stands out for its exceptional properties, having great significance in both fundamental physics and the electronics industry.[5−11] For a range of promising applications, interfacing graphene with metals is a necessary and crucial process.[12] In electronic device integration, making electrical contact between graphene and metal electrodes, typically achieved through thermal or electron beam evaporation, is a fundamental step critical to the success of subsequent fabrication processes. High contact resistance often introduces limitations on the actual performance of graphene-based devices.[13] Numerous theoretical and experimental studies have been reported on the interfaces of various metals with graphene.[14−16] Here, we report an interesting observation regarding changes in optical contrast when depositing 10−12 nm of various metals onto chemical vapor deposition (CVD) synthesized graphene and attribute this to interfacial oxidation. This oxidation process at the metal−graphene interface has not been investigated before and should

Received: July 25, 2024
Revised: October 2, 2024
Accepted: October 10, 2024
Published: October 23, 2024

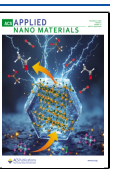

© 2024 American Chemical Society

https://doi.org/10.1021/acsanm.4c04283
ACS Appl. Nano Mater. 2024, 7, 24537−24546

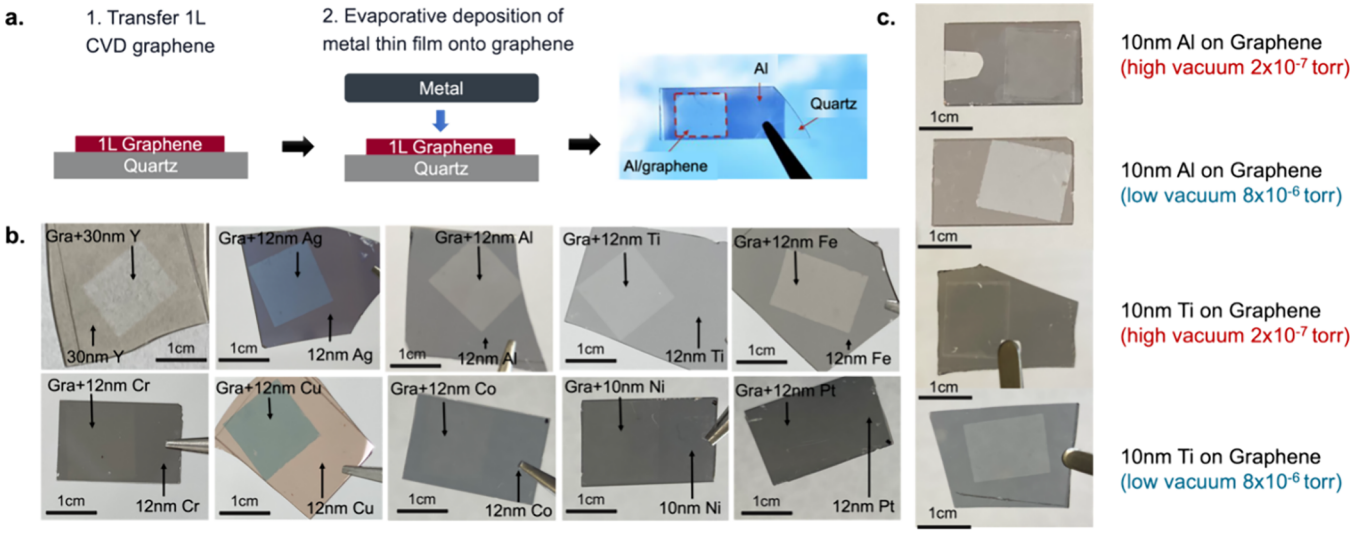

Figure 1. (a) Schematic diagram of the metal thin film deposited on graphene. Graphene (grown by CVD) was transferred on transparent quartz substrate, and then 10−12 nm thin metal film is deposited. On the right is a photograph of 12 nm of Al deposited on graphene. The area on top of graphene appears more transparent. (b) Photographs of various metals deposited onto graphene (vacuum level at 8×10^{-6} Torr for all samples). Metals including Y, Ag, Al, Ti, Fe, Cr, and Cu show noticeable change in optical contrast for the area on top of graphene, while for Co, Ni, and Pt, the optical contrast are less clearly visible. (c) Different changes in transparency as Al or Ti were deposited under different vacuum levels.

provide valuable insights into the properties of metal−graphene interfaces and the process associated with metal deposition on graphene.

In our experimental setup, we deposited aluminum (Al) with thickness ranging from 5 to 20 nm using an electron beam evaporator onto a quartz substrate, over which a square-shaped graphene sheet had been transferred prior to the deposition. We observed that when the thickness of Al is between 10 and 12 nm, there is an obvious difference in transparency in the region with graphene vs the region directly deposited on the substrate, immediately after the sample was taken out of the deposition chamber, as shown in Figure 1a. This difference is less obvious when the thickness of Al is less than 10 nm or more than 12 nm. Therefore, we further extended our investigation to additional nine metals including platinum (Pt), cobalt (Co), nickel (Ni), chromium (Cr), copper (Cu), titanium (Ti), iron (Fe), yttrium (Y), and silver (Ag). For each metal, we deposited 10−12 nm in thickness onto graphene. We found that, for certain metals such as Ti, Fe, and Ag, a noticeable difference in transparency or color is shown for the region on top of graphene vs the region directly on the substrate (Figure 1b). Conversely, for other metals, including Ni, Co, and Pt, the optical differences were barely noticeable, as shown in Figure 1b. Additionally, we noted that when deposition proceeds under high vacuum ($\lesssim 2\times10^{-7}$ Torr), the optical differences for 10 nm Al on graphene and 10 nm Ti on graphene become considerably less. Particularly for Ti, the difference becomes unnoticeable, as shown in Figure 1c.

To elucidate the causes of the change in optical contrast, we studied the metal−graphene interface structure in evaporated Al, Ti, and Ni. We employed a range of analytical techniques, including XPS, XRR, Raman spectroscopy, UV−vis transmittance, and sheet resistance measurement. We will show below that the change in transparency observed in Al-graphene and Ti-graphene comes from interfacial oxidation at the metal−graphene interface, resulting in the formation of a metal oxide layer. In contrast, we did not observe interfacial oxidation at the Ni-graphene interface, aligning with its indistinct change in transparency. We propose a model based on the metal work function and interaction with graphene to offer insights into identifying metals prone to interfacial oxidation, and we discuss the role of the background vacuum level during deposition in determining the extent of oxide formation.

RESULTS

From the group of metals in Figure 1b, we present detailed studies of Al, Ti, and Ni as representative of the behaviors we observed. We compare Al deposited on graphene, which shows an enhancement in transparency, with Ni deposited on graphene, which does not. We selected Ti because the results are sensitive to the vacuum level in the chamber: the enhancement of transparency is observed in low vacuum and becomes minimal when deposited under high vacuum (Figure 1c).

A 10 nm Al is deposited using electron beam evaporation onto CVD-grown graphene on a transparent quartz substrate (growth and transfer method in Supporting Information). The deposition is conducted using a closed chamber evaporator with nitrogen as backfill gas (Ebeam Temescal- LL, Mode: Temescal FC2000. It provides base pressure up to 2×10^{-7} Torr with >1 h pumping down. The deposition rate is controlled to be 0.5 Å/s at room temperature (details in the Supporting Information). The difference in transparency for the regions on and off graphene is observed immediately after deposition. To find out whether there is a change over time in the ambient environment, we measured UV−visible transmittance over 560 days. As shown in Figure 2a and Figure S1a, the difference in transmittance increases from 7.5 to 18% after 35 days and to 23.8% after 561 days, while the transmittance of the region that is directly on the substrate increases much slower. The sheet resistance of the region above graphene increases more than five times (from 42 to 234 Ω/square) after 237 days and keeps increasing over a longer period (Figure 2b, Figure S8). X-ray reflectivity (XRR) was measured on the sample right after deposition and suggests an α-Al_2O_3−Al-

https://doi.org/10.1021/acsanm.4c04283
ACS Appl. Nano Mater. 2024, 7, 24537−24546

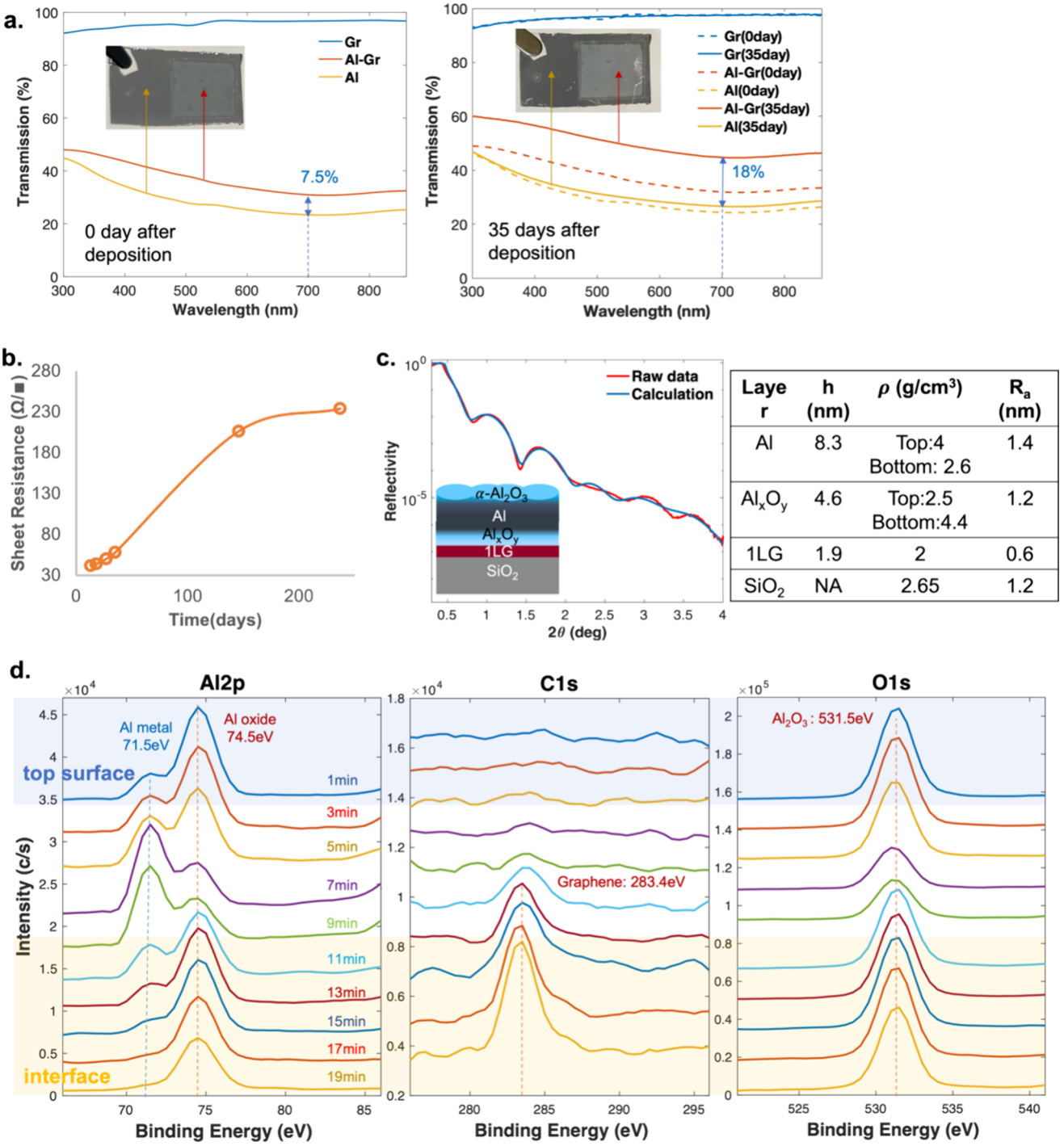

Figure 2. Characterizations for 10 nm Al deposited on graphene. (a) UV−vis transmittance (300−850 nm) measured over a period of 35 days, the second graph overlays signal from 0 day (dashed lines) and 35 days (solid lines), both calibrated according to transmittance of CVD-grown graphene (insets: photographs of Al-graphene-quartz sample, brighter square region contains graphene). (b) Sheet resistance measured over time. (c) XRR profile with simulated layered structure, with the top two layers modeled with linear gradient density. The inserted table shows detailed information on each layer. The first layer with density from the top 4 to bottom 2.6 g/cm^3, indicating a transition from α-Al_2O_3 (3.99 g/cm^3) to Al (2.7 g/cm^3). Meanwhile, the second layer's density is at the top 2.5 g/cm^3 and the bottom 4.4 g/cm^3, indicating a transition from Al to Al_xO_y. ρ: density; h: thickness; R_a, roughness. (d) XPS depth profile by Ar ion sputtering (sputtering time marked at each curve).

Al_xO_y-graphene structure (Figure 2c). To further examine the interface structure, we measured the XPS depth profile on the same sample. The sample was sputtered with an Ar ion gun, and signals for Al 2p, C 1s, and O 1s orbitals were collected at each round. The information depth for this sample is around 3 nm,[17] and the sputtering rate is roughly 0.5 nm/min. As shown in Figure 2d, the surface initially shows strong Al oxide and oxygen peaks. As sputtering continues, the aluminum oxide peaks decrease, while Al metal peaks increase. The oxygen peak also decreases, indicating a region dominated by the Al metal. However, as the sputtering continues, the Al metal peak decreases and finally disappears, while the Al oxide peak and

https://doi.org/10.1021/acsanm.4c04283
ACS Appl. Nano Mater. 2024, 7, 24537−24546

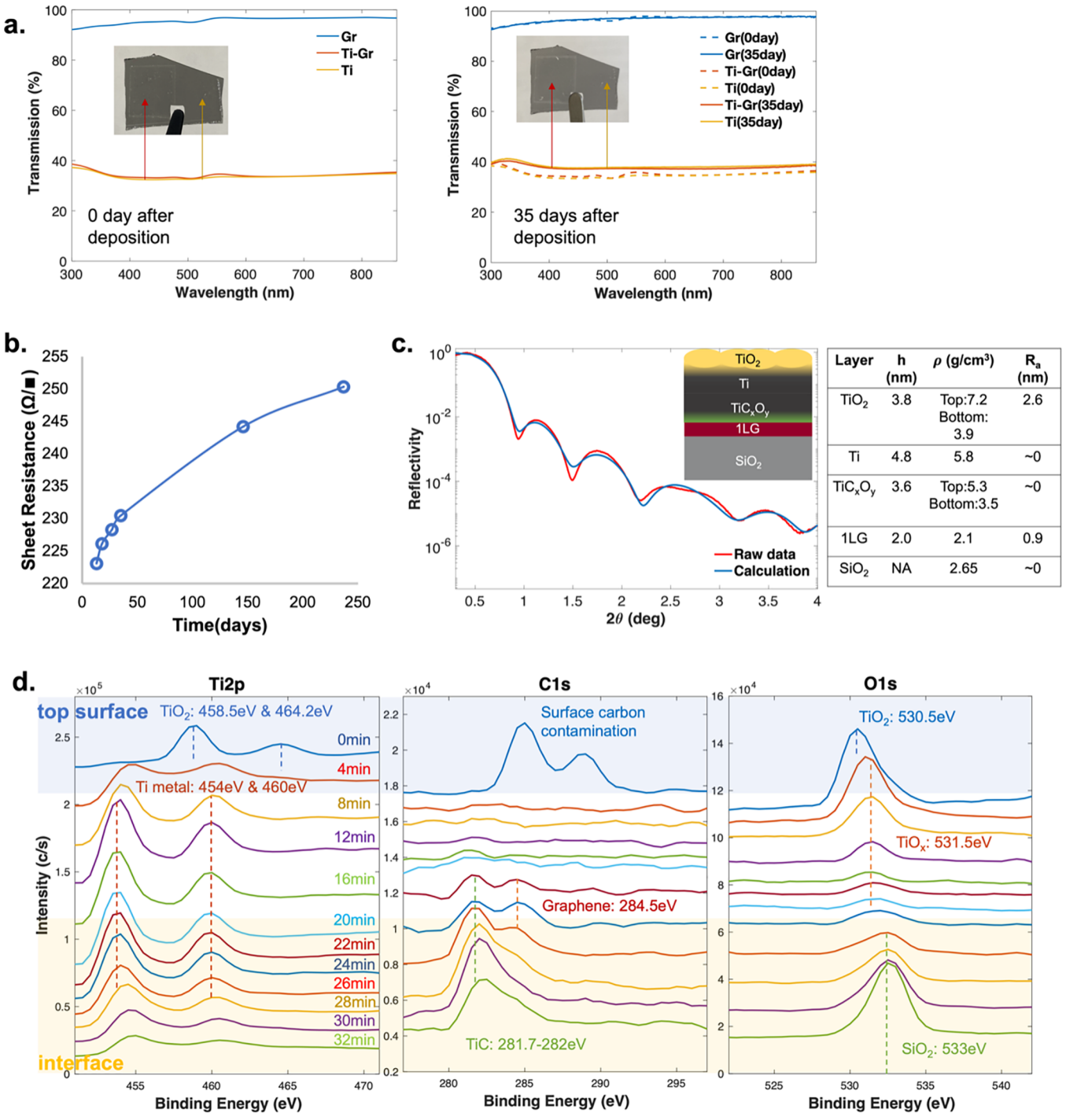

Figure 3. Characterizations for 10 nm Ti on graphene deposited under high vacuum (2×10^{-7} Torr) (insets: photographs of Ti-graphene-quartz sample, square region on the left is graphene). (a) UV−vis transmittance (300−850 nm) measured over time, the second graph overlays signal from 0 (dashed lines) to 35 days (solid lines), both calibrated according to transmittance of CVD-grown graphene. (The UV−vis transmittance for Ti/graphene/quartz and Ti/quartz shows minimal difference, and the transmittance is <3% higher over 35 days.) (b) Sheet resistance measured over 35 days. (c) XRR profile with simulated layered structure, first and third layers modeled with linear gradient density. The inset table shows information for each layer. ρ, density; h: thickness; R_a: roughness. (d) XPS depth profile by Ar ion sputtering (sputtering time marked at each curve).

oxygen peak increase in intensity. Meanwhile, the carbon peak for graphene emerges, which indicates that the sputtering has reached the Al-graphene interface. From the XPS depth profile, it is clear that for the film on top of graphene the Al underneath the surface Al oxide layer is not pure Al but has noticeable oxide content, especially when it is closer to the Al/graphene interface. This is in contrast to the XPS depth profile of the 10 nm Al deposited on quartz as further discussed in the Supporting Information (Figure S2). To eliminate the influence of surface oxidation of Al, we deposited 5 nm Ni on top of 10 nm Al on graphene in the same chamber to prevent oxidation from the surface. Ni is chosen as a protection

https://doi.org/10.1021/acsanm.4c04283
ACS Appl. Nano Mater. 2024, 7, 24537−24546

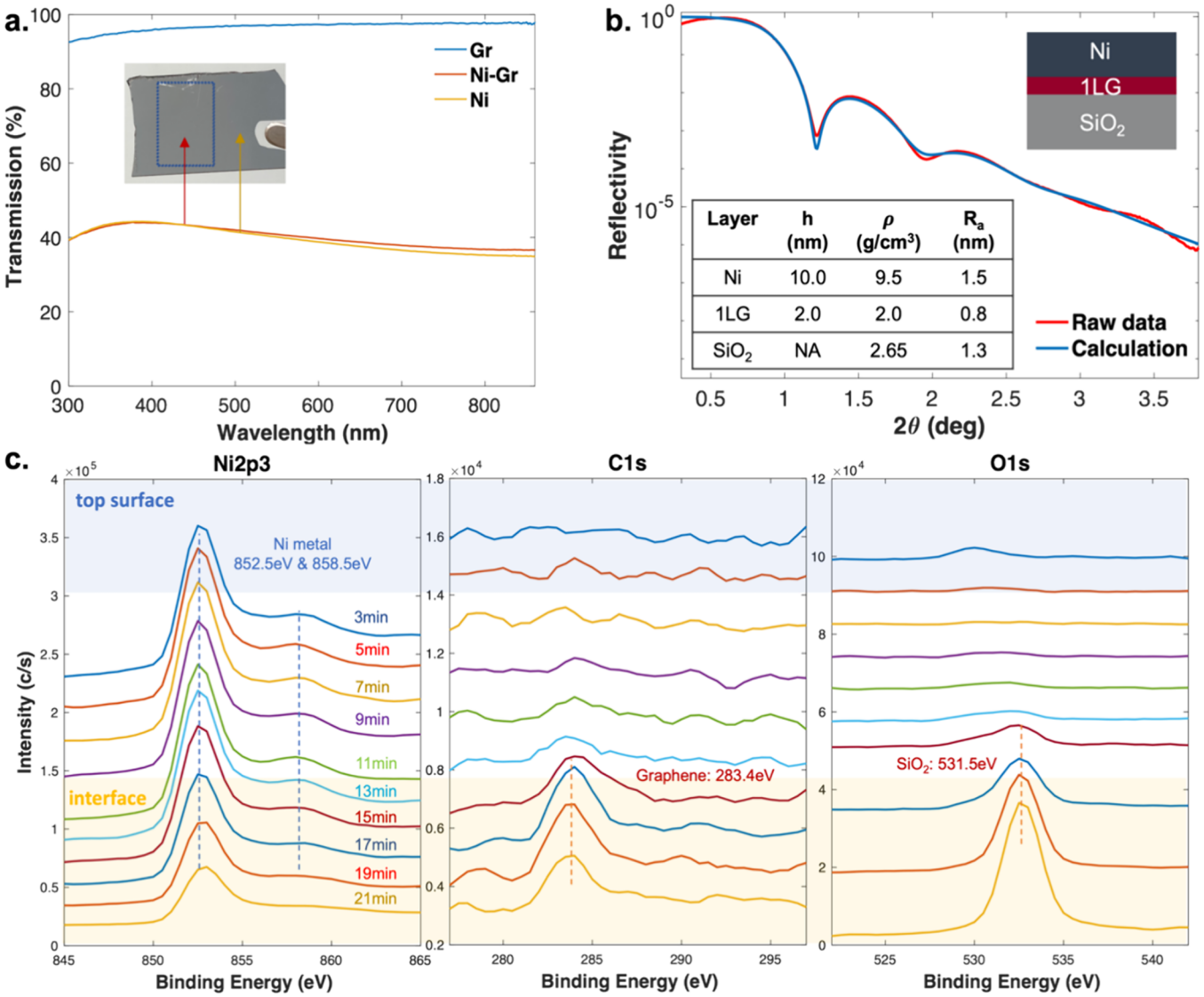

Figure 4. Characterizations for 10 nm Ni deposited on graphene. (a) UV−vis transmittance (300−850 nm) of 10 nm Ni on graphene on quartz and 10 nm Ni on quartz (inset: photograph of Ni-graphene-quartz sample, square region outlined contains graphene). (b) XRR profile with the predicted layered structure. The table inserted shows detailed information on each layer. ρ: density; h: thickness; R_a: roughness. (c) XPS depth profile by Ar ion sputtering (sputtering time marked at each curve).

layer since in our later experiment for Ni deposition on graphene, we did not observe the oxidation of Ni. The XPS depth profile and XRR both imply a Ni−Al−Al_xO_y-graphene structure (Figure.S3). These results suggest that the change in transparency for the region on top of graphene is due to interface oxidation, and the oxidation appears to continue in an ambient environment but slows over time. This oxidation behavior appears to differ from the formation of surface α-Al_2O_3 of Al in air, since the surface α-Al_2O_3 is dense, which prevents Al from being further oxidized, as typically there is no continuation of oxidation over time. To measure the thickness of the interfacial Al_xO_y layer, we conducted cross-sectional atomic-resolution transmission electron microscopy (TEM) analysis on samples of 10 nm Al followed by 5 nm Ni deposited on graphene (deposition at 2×10^{-7} Torr). The electron energy loss spectroscopy (EELS) mapping of the elements Al, O, and C within the cross-sectional region reveals the presence of an oxide layer, approximately 5 nm in thickness, above the graphene (Figure S4)

We now discuss the Ti-graphene interface formed after the evaporation of 10 nm Ti on graphene. As observed in Figure 1c, the deposition of Ti is highly sensitive to the vacuum level. Thus, we performed deposition under three vacuum levels: 2×10^{-7} (high vacuum), 2×10^{-6} (mid vacuum), and 8×10^{-6} Torr (low vacuum). Different vacuum levels are controlled by varying the time of pumping down before the deposition (experimental details in the Supporting Information). Figure 3 shows the sample deposited under high vacuum, while the samples deposited at 2×10^{-6} and 8×10^{-6} Torr (mid and low vacuum) are included in Figures S5 and S6, respectively. When deposited under a high vacuum, the region that is on top of graphene has roughly the same transmittance as the region directly on the substrate. No change in transparency is visible after the sample is left in the air for 35 days, and we measured only a 3.4% difference in transparency after 561 days (Figure 3a, Figure S1b). The sheet resistance of the region containing graphene increases only 12% (from 223 to 250 Ω/square) after 237 days in the ambient environment (Figure 3b). We first

https://doi.org/10.1021/acsanm.4c04283
ACS Appl. Nano Mater. 2024, 7, 24537−24546

collected XRR information for the sample right after deposition (Figure 3c). Then, the XPS profile is collected for the Ti 2p, C 1s, and O 1s lines, at a sputtering rate of around 0.3 nm/min, as shown in Figure 3d, which indicates the TiO_2 layer on top of Ti metal. At the interface, the C 1s signal shows a strong peak at 281.5 eV, which is distinct from the graphene peak at 284.5 eV. This peak is identified as carbide, indicating the formation of TiC during deposition. For this high vacuum condition, even without a clear transparency contrast, the O 1s XPS and XRR data still indicated a small amount of oxidation. We conclude that 10 nm Ti on graphene has a sandwich structure: TiO_2−Ti-TiC_xO_y, with the majority being TiC and a trace amount of oxide at the Ti-graphene interface.

For Ti deposited on graphene under conditions in which the base pressure in the chamber is higher during deposition, the region deposited on top of the graphene appears more transparent (Figure 1(b)). When Ti is deposited under 2×10^{-6} Torr, the region containing graphene is 4.6% higher in transparency. The difference increases to 12.11% after 534 days (Figure S1(c)). When deposited under 8.6×10^{-6} Torr, the region deposited on top of the graphene is even more transparent with a difference of 6.2% in transparency right after Ti deposition. The difference increases to 16.6% after 512 days (Figure S1d). In both cases, XRR results indicate a structure of TiO_2−TiC_xO_y-graphene (Figures S5b and S6b). Also, the XPS depth profile shows a strong O 1s signal throughout the thickness of the Ti layer, implying that Ti becomes partially oxidized during the deposition (Figures S5c and S6c). Apart from these two vacuum conditions, we also deposited Ti on graphene at a vacuum level of 5×10^{-7} Torr. We collected XPS depth profiles on two adjacent spots, on-graphene and off-graphene, on the same sample of 10 nm Ti deposited on graphene on a quartz substrate. As shown in Figure S7, Ti is partially oxidized when deposited on graphene, which is not the case if deposited on quartz, and the degree of Ti oxidation on the graphene is intermediate between the high vacuum (2×10^{-7} Torr) and medium vacuum (2×10^{-6} Torr) conditions. To summarize the case of Ti, the transparency contrast is more sensitive to the vacuum levels than that found for Al. For Ti, clear transparency contrast was only observed in lower vacuum conditions ($\geq 5 \times 10^{-7}$ Torr), but from O 1s XPS depth profiles, there is always oxidation, which increases as the vacuum level degrades.

To compare with Al and Ti, we studied the interface structure of 10 nm Ni deposited on graphene. The region on top of graphene shows negligible enhancement in UV−vis transmittance as compared to the region directly on the substrate, whether Ni is deposited under high or low vacuum levels (Figure 4a at 2×10^{-7} Torr, Figure 1c at 8.6×10^{-6} Torr). XPS profile and XRR results both indicate a sharp transition from the Ni metal layer to the graphene layer, without an oxide layer at the interface (Figure 4b,c).

To understand the different behaviors when Al, Ti, and Ni are deposited on graphene, we looked into the intrinsic properties of metals and their interactions with graphene. The interaction of metals with graphene has been categorized into physisorption and chemisorption.[14] Physisorption is a weaker interaction with low absorption energy (0.03−0.05 eV per carbon), and the equilibrium interfacial distance is >3.0 Å. Chemisorption is a strong interaction with an equilibrium interfacial distance of <2.5 Å and higher adsorption energy (0.09−0.4 eV per carbon), due to the substantial overlap between the wave functions of d electrons in the metal and π electrons in graphene.[14] As shown in Table 1, Al, Ag, and Pt are categorized as physisorbed metals, which interact with graphene through a relatively weak van der Waals force. Also, Ti, Ni, and Co are categorized as chemisorbed metals.[14,18,19] This aligns well with our Raman results, which are also consistent with the literature.[20] We measured the Raman spectrum before and after deposition for 10 nm Al, Ti, and Ni on graphene. Deposition of Al causes a minor change in the G and 2D peaks, implying weak interaction. In contrast, the deposition of Ni or Ti induces a significant decrease in intensity on both peaks, especially the 2D peak, which implies a strong interaction with graphene (Figure 5a,b).

Table 1. Binding Energies (E_b), Equilibrium Atomic Distances (D_{eq}), and Work Function (W_F) of Various Metals with Graphene[a]

type	metals	E_b (eV/atom)	D_{eq} (Å)	W_F (eV)
physisorbed	Al	0.027	3.59	4.28
physisorbed	Ag	0.043	3.26	4.26
physisorbed	Cu	0.033	2.96	4.65
physisorbed	Pt	0.038	3.18	5.65
chemisorbed	Ti	0.327	2.13	4.33
chemisorbed	Ni	0.125	2.07	5.15
chemisorbed	Co	0.160	2.11	5.0

[a]Data taken from references: interaction types,[14] binding energies (E_b),[18,19] equilibrium atomic distances (D_{eq}),[14] and work function (W_F).[21]

DISCUSSION

By considering both the work function of the metal relative to that of graphene and the type of interaction occurring between the metal and graphene, we propose the following mechanism (Figure 5c,d). During the deposition process, for metals with a work function lower than that of graphene, such as Al, there is charge transfer between the metal and the graphene, causing the metal to be electron-deficient while graphene to be doped n-type. Since graphene adsorbs oxygen and water from the ambient,[22−25] under a relatively low background vacuum level ($1-8 \times 10^{-6}$ Torr), part of the adsorbed water and oxygen molecules remain on the graphene surface and form oxygen anions. Since physisorbed metals have poor wettability on graphene, the metal follows island growth after nucleation.[26,27] Before graphene is fully covered with metal, the oxygen anions absorbed on graphene react with the metal that contacts graphene, which is electron-deficient, and forms an interfacial metal oxide. The amount of oxidation becomes less as the deposition continues (likely because the distance is larger from the graphene surface), and the film that forms is a mixture of the metal and metal oxide (as indicated by the XPS depth profile and XRR data). Once the sample is taken out of the vacuum chamber, it appears that the interfacial oxidized layer is not as dense as the typical surface oxidation layer (e.g., α-Al_2O_3), and the oxidation still continues for a period of time. Since the oxidation of metal atoms leads to changes in light absorption in the visible regime, the interfacial oxidation layer causes a noticeable change in optical contrast, which is observed for Ti, Ag, Fe, and Al. For Ti, since it is a chemisorbed metal on graphene with a lower work function, this process is highly dependent on the vacuum condition. We expect that the oxidation of Ti on graphene, which happens at lower vacuum conditions, goes through a similar mechanism as

https://doi.org/10.1021/acsanm.4c04283
ACS Appl. Nano Mater. 2024, 7, 24537−24546

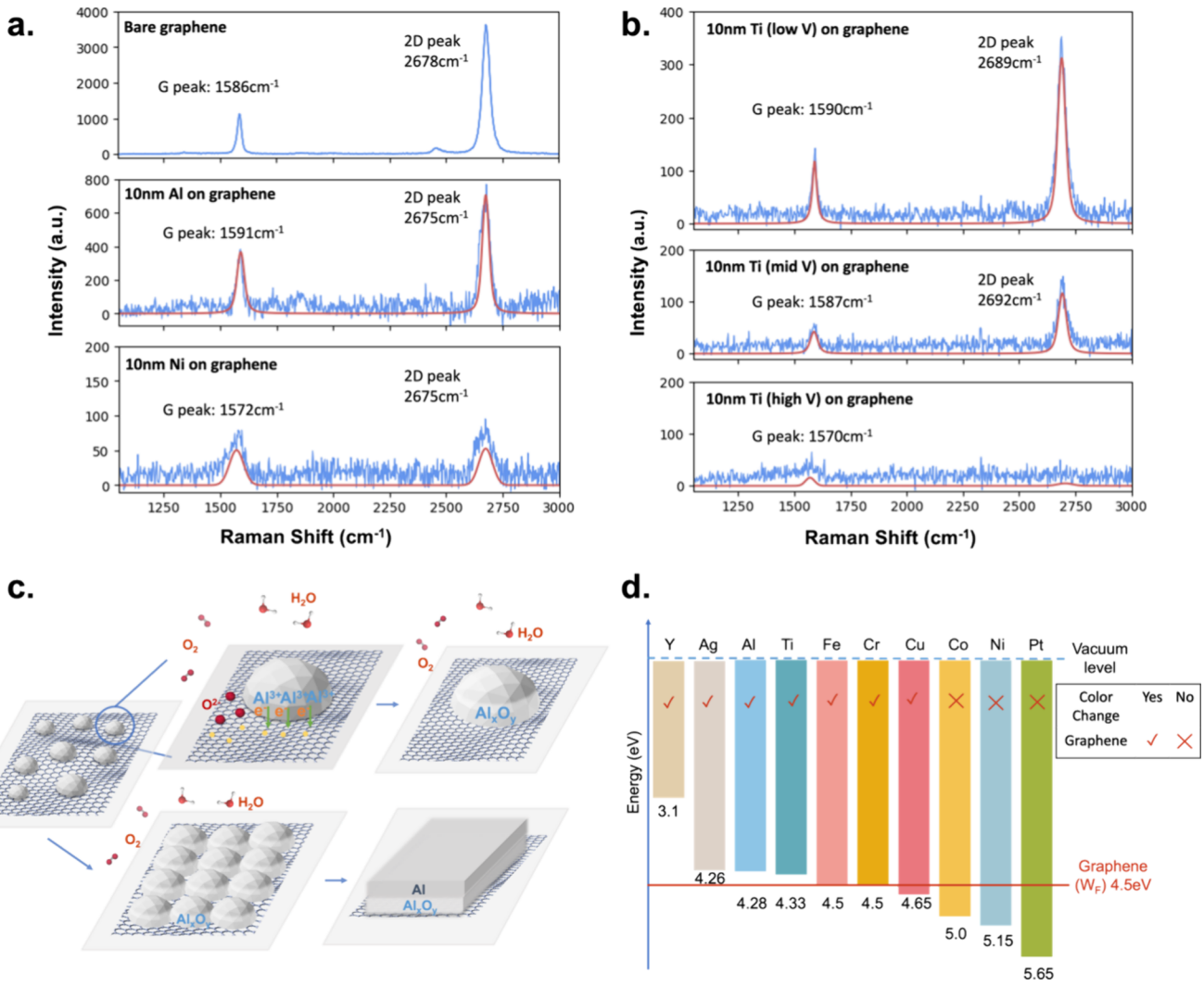

Figure 5. (a) Raman spectra for bare graphene, 10 nm Al on graphene and 10 nm Ni on graphene (vacuum level during deposition: 2×10^{-7} Torr). (b) Raman spectra for 10 nm Ti on graphene, deposited under different vacuum levels (from top to bottom: low V: 8×10^{-6} Torr; mid V: 2×10^{-6} Torr; high V: 2×10^{-7} Torr). (c) Illustration of our proposed graphene-enhanced interfacial oxidation mechanism: the top route shows the charge transfer and oxidation process of a single metal island on graphene, while the bottom route shows that during deposition all metal islands that are contacting graphene get oxidized, resulting in formation of an interfacial metal oxide film on graphene. (d) Energy diagram of 10 metals work function with regards to the work function of graphene,[21] and the indication of whether color change is observed when metal is deposited on graphene.

proposed in Figure 5c. However, at higher vacuum, surface-induced hybridization between Ti and graphene is observed rather than the oxidation of Ti at the interface. In Figure 5d, we plot the work functions of various metals in comparison to graphene's work function. When the metal's work function is lower than graphene's, charge transfer happens at the interface, which causes the metal to be electron-deficient. The previously adsorbed oxygen on graphene could serve as the oxidation source (the amount of oxygen should also depend on the base pressure in the chamber), and metal could be oxidized by taking up the oxygen from the graphene's surface. The possible atomic-scale processes involved can be (1) when a metal atom is contacting graphene, due to the difference in work function, charge transfer happens via the move of electrons and holes, leaving the metal atom positively charged and (2) the adsorbed oxygen on graphene's surface (no bond formation with graphene) got taken up by metal atom and forms an M−O bond. Both hypothesized processes are illustrated in Figure 5c. For metals with a work function higher than that of graphene, such as Pt and Ni, such a metal oxidation process would not occur, which is consistent with our observation of no obvious change in optical contrast.

For Al, it has been reported that when depositing 1−2 nm Al on graphene using electron beam deposition, the Al layer is quickly oxidized, and serves as a nucleation layer that enables atomic layer deposition (ALD) of Al_2O_3.[28] However, the role of graphene in enabling this oxidation has not previously been discussed. Based on our analysis, during the deposition of the metal film in the chamber, graphene facilitates the oxidation of Al through charge transfer, resulting in an interfacial Al_xO_y layer. For the deposition of Ti on graphene, our results suggest that the interaction between graphene and metal plays a significant role, which leads to higher sensitivity to the vacuum level during deposition. Under relatively high vacuum level (2×10^{-7} Torr) (Figure 3), due to the strong interaction between graphene and Ti, surface-induced hybridization occurs, and there is minimal oxidation at the interface between Ti and graphene. As shown in Figure 5a,b, the attenuation of

https://doi.org/10.1021/acsanm.4c04283
ACS Appl. Nano Mater. 2024, 7, 24537−24546

graphene's G and 2D peaks is due to the strong interaction between Ti atoms and graphene, which broadens the G peak and quenches the 2D peak. This is consistent with the previous study on Ti-graphene hybridization, in which both G and 2D peaks reappear after etching away the Ti with HF. This indicates that graphene is not damaged during deposition.[29] However, as the vacuum level becomes lower (which means that there is more oxygen or H_2O in the chamber), interfacial oxidation takes over. This can also be observed in the change of the Raman spectrum under different vacuum levels (in Figure 5b, under high vacuum level, due to the strong interaction between graphene and Ti, there is a large downshift, broadening of the graphene G peak, and quenching of the 2D peak; while the G peak and 2D peak gradually recover as the vacuum level worsens). We also note that the C 1s spectrum from the XPS depth profile shows both TiC and graphene at the interface, as also observed in other reports of Ti deposition on graphene.[29,30] It is highly possible that the TiC signal is a result of the reaction of Ti with the residual gas in the deposition chamber as well as polymer contamination on the graphene surface, rather than a direct reaction with graphene.[29−31] This explains the observation that at a lower vacuum level, which implies a higher concentration of background gas, the TiC peak appears earlier in the depth profiling than the graphene peak (Figures S5 and S6). For the deposition of Ni onto graphene, this process appears to be insensitive to the vacuum level during deposition. We did not observe a change in transparency for the area containing graphene, nor the formation of carbide or oxide layers at the Ni-graphene interface (Figures 1b and 4). This can be understood by the high work function of Ni in comparison with Al and Ti. Under relatively high base pressure (8.6×10^{-6} Torr), Ni does not oxidize as easily as Al and Ti.

CONCLUSIONS

In conclusion, our study has revealed a phenomenon involving a change in transparency when depositing 10−12 nm of metals onto graphene that was transferred on a transparent substrate. To understand this phenomenon, we focused on aluminum, titanium, and nickel to study their interactions with graphene. Our findings collectively point to the formation of an interfacial oxide layer at the metal−graphene interface as the cause of the observed changes in transparency. Our model and observation show that the metal work function and type of interaction with graphene act as a guide to determine whether interfacial oxidation is expected and whether deposition conditions strongly influence the extent of oxide formation. For the case that interfacial oxidation is not desirable, we suggest careful in situ baking before deposition to remove the adsorbed gas molecules on graphene and the use of an ultrahigh vacuum deposition tool to avoid oxidation. While this metal−metal oxide-graphene structure is promising, particularly in the case of forming tunnel barrier contacts for graphene channel devices. Graphene's long spin-diffusion length at room temperature makes it a standout choice for spintronic devices.[32] During the fabrication process, it is often necessary to form tunnel barrier contacts for the injector and detector magnets. This study elucidates the formation of interfacial oxide layers, which is highly relevant when optimizing tunnel barrier contacts for graphene spin channel devices. For Al, the use of interfacial oxide has already been demonstrated in graphene transistors,[33] and in carbon nanotube transistors using graphene as a cold-source contact and Al as a gate electrode.[34] This study, therefore, contributes valuable insights whenever metal is deposited onto graphene for different device fabrications.

ASSOCIATED CONTENT

Supporting Information

The Supporting Information is available free of charge at https://pubs.acs.org/doi/10.1021/acsanm.4c04283.

(1) Experimental methods; (2) UV−vis transmittance (300−850 nm) for 0−561 days after deposition of Al/Ti on graphene; (3) XPS depth profile for 10 nm Al deposited on quartz substrate vs 10 nm Al deposited on graphene; (4) characterizations for 10 nm Al + 5 nm Ni deposited on graphene at relatively low vacuum level; (5) cross-sectional HR-TEM and EELS mapping, of 10 nm Al following 5 nm Ni deposited on graphene; (6) characterizations of Ti on graphene deposited at mid vacuum level and (7) low vacuum level; (8) XPS depth profile for 10 nm Ti deposited on quartz substrate vs 10 nm Ti deposited on graphene; and (9) change of sheet resistance for 10 nm Al on graphene and 10 nm Ti on graphene over 570 days (PDF)

AUTHOR INFORMATION

Corresponding Author

Jing Kong − *Department of Electrical Engineering and Computer Science, Massachusetts Institute of Technology, Cambridge, Massachusetts 02139, United States;* orcid.org/0000-0003-0551-1208; Email: jingkong@mit.edu

Authors

Zhien Wang − *Department of Electrical Engineering and Computer Science and Department of Materials Science and Engineering, Massachusetts Institute of Technology, Cambridge, Massachusetts 02139, United States;* orcid.org/0000-0002-6120-1952

Haozhe Wang − *Department of Electrical and Computer Engineering, Duke University, Durham, North Carolina 27708, United States;* orcid.org/0000-0001-5123-1077

Roman Caudillo − *Semiconductor Research Cooperation, Durham, North Carolina 27703, United States; Intel Laboratories, Intel Corporation, Hillsboro, Oregon 97124, United States*

Jiangtao Wang − *Department of Electrical Engineering and Computer Science, Massachusetts Institute of Technology, Cambridge, Massachusetts 02139, United States;* orcid.org/0000-0001-7323-4690

Zhenjing Liu − *Department of Materials Science and Engineering, Massachusetts Institute of Technology, Cambridge, Massachusetts 02139, United States;* orcid.org/0000-0003-4020-1774

Alexandre Foucher − *Department of Materials Science and Engineering, Massachusetts Institute of Technology, Cambridge, Massachusetts 02139, United States;* orcid.org/0000-0001-5042-4002

Ji-Hoon Park − *Department of Electrical Engineering and Computer Science, Massachusetts Institute of Technology, Cambridge, Massachusetts 02139, United States*

Meng-Chi Chen − *Department of Electrical Engineering and Computer Science, Massachusetts Institute of Technology, Cambridge, Massachusetts 02139, United States*

https://doi.org/10.1021/acsanm.4c04283
ACS Appl. Nano Mater. 2024, 7, 24537−24546

Ang-yu Lu − *Department of Electrical Engineering and Computer Science, Massachusetts Institute of Technology, Cambridge, Massachusetts 02139, United States*
Peng Wu − *Department of Electrical Engineering and Computer Science, Massachusetts Institute of Technology, Cambridge, Massachusetts 02139, United States;* orcid.org/0000-0001-9866-0450
Jiadi Zhu − *Department of Electrical Engineering and Computer Science, Massachusetts Institute of Technology, Cambridge, Massachusetts 02139, United States*
Xudong Zheng − *Department of Electrical Engineering and Computer Science, Massachusetts Institute of Technology, Cambridge, Massachusetts 02139, United States*
Tymofii S. Pieshkov − *Department of Materials Science and NanoEngineering and Applied Physics Graduate Program, Smalley-Curl Institute, Rice University, Houston, Texas 77005, United States*
Steven A. Vitale − *Lincoln Laboratory, Massachusetts Institute of Technology, Lexington, Massachusetts 02421, United States;* orcid.org/0000-0002-6035-018X
Yimo Han − *Intel Laboratories, Intel Corporation, Hillsboro, Oregon 97124, United States;* orcid.org/0000-0003-0563-4611
Frances M. Ross − *Department of Materials Science and Engineering, Massachusetts Institute of Technology, Cambridge, Massachusetts 02139, United States;* orcid.org/0000-0003-0838-9770
Iwnetim I. Abate − *Department of Materials Science and Engineering, Massachusetts Institute of Technology, Cambridge, Massachusetts 02139, United States*

Complete contact information is available at: https://pubs.acs.org/10.1021/acsanm.4c04283

Author Contributions

The manuscript was written through contributions of all authors. All authors have given approval to the final version of the manuscript.

Notes

The authors declare no competing financial interest.

■ ACKNOWLEDGMENTS

This work was supported in part by the Semiconductor Research Corporation Center 7 in JUMP 2.0 (award no. 145105-21913). J.W. and J.K. acknowledge financial support from the Air Force Office of Scientific Research (AFOSR) Multi-University Research Initiative FA9550-22-1-0166, X.Z. and J.K. acknowledge the support by the US Army Research Office grant number W911NF2210023. T.P. and Y.H. acknowledge the support from NSF (CMMI−2239545), Welch Foundation (C-2065), and American Chemical Society Petroleum Research Fund (67236-DNI10). This work made use of the Shared Experimental Facilities, supported in part by the MRSEC Program of the National Science Foundation under award number DMR-1419807, and MIT.Nano's facilities.

■ REFERENCES

(1) Novoselov, K. S.; Geim, A. K.; Morozov, S. V.; Jiang, D.; Zhang, Y.; Dubonos, S. V.; Grigorieva, I. V.; Firsov, A. A. Electric Field Effect in Atomically Thin Carbon Films. *Science* **2004**, *306* (5696), 666−669.
(2) Novoselov, K. S.; Jiang, D.; Schedin, F.; Booth, T. J.; Khotkevich, V. V.; Morozov, S. V.; Geim, A. K. Two-Dimensional Atomic Crystals. *Proc. Natl. Acad. Sci. U.S.A.* **2005**, *102* (30), 10451−10453.
(3) Geim, A. K.; Novoselov, K. S. The Rise of Graphene. *Nanoscience and technology: a collection of reviews from nature journals.* **2009**, 11−19.
(4) Khan, K.; Tareen, A. K.; Aslam, M.; Wang, R.; Zhang, Y.; Mahmood, A.; Ouyang, Z.; Zhang, H.; Guo, Z. Recent Developments in Emerging Two-Dimensional Materials and Their Applications. *J. Mater. Chem. C* **2020**, *8* (2), 387−440.
(5) Balandin, A. A.; Ghosh, S.; Bao, W.; Calizo, I.; Teweldebrhan, D.; Miao, F.; Lau, C. N. Superior Thermal Conductivity of Single-Layer Graphene. *Nano Lett.* **2008**, *8* (3), 902−907.
(6) Lee, C.; Wei, X.; Kysar, J. W.; Hone, J. Measurement of the Elastic Properties and Intrinsic Strength of Monolayer Graphene. *Science* **2008**, *321* (5887), 385−388.
(7) Bolotin, K. I.; Sikes, K. J.; Jiang, Z.; Klima, M.; Fudenberg, G.; Hone, J.; Kim, P.; Stormer, H. L. Ultrahigh Electron Mobility in Suspended Graphene. *Solid State Commun.* **2008**, *146* (9), 351−355.
(8) Nair, R. R.; Blake, P.; Grigorenko, A. N.; Novoselov, K. S.; Booth, T. J.; Stauber, T.; Peres, N. M. R.; Geim, A. K. Fine Structure Constant Defines Visual Transparency of Graphene. *Science* **2008**, *320* (5881), 1308−1308.
(9) Bonaccorso, F.; Sun, Z.; Hasan, T.; Ferrari, A. C. Graphene Photonics and Optoelectronics. *Nature Photon* **2010**, *4* (9), 611−622.
(10) Novoselov, K. S.; Fal'ko, V. I.; Colombo, L.; Gellert, P. R.; Schwab, M. G.; Kim, K. A Roadmap for Graphene. *Nature* **2012**, *490* (7419), 192−200.
(11) Tiwari, S. K.; Sahoo, S.; Wang, N.; Huczko, A. Graphene Research and Their Outputs: Status and Prospect. *Journal of Science: Advanced Materials and Devices* **2020**, *5* (1), 10−29.
(12) Yang, M.; Liu, Y.; Fan, T.; Zhang, D. Metal-Graphene Interfaces in Epitaxial and Bulk Systems: A Review. *Prog. Mater. Sci.* **2020**, *110*, No. 100652.
(13) Venugopal, A.; Colombo, L.; Vogel, E. M. Contact Resistance in Few and Multilayer Graphene Devices. *Appl. Phys. Lett.* **2010**, *96* (1), No. 013512.
(14) Gong, C.; Lee, G.; Shan, B.; Vogel, E. M.; Wallace, R. M.; Cho, K. First-Principles Study of Metal−Graphene Interfaces. *J. Appl. Phys.* **2010**, *108* (12), No. 123711.
(15) Lazar, P.; Zhang, S.; Šafářová, K.; Li, Q.; Froning, J. P.; Granatier, J.; Hobza, P.; Zbořil, R.; Besenbacher, F.; Dong, M.; Otyepka, M. Quantification of the Interaction Forces between Metals and Graphene by Quantum Chemical Calculations and Dynamic Force Measurements under Ambient Conditions. *ACS Nano* **2013**, *7* (2), 1646−1651.
(16) Shin, S. E.; Choi, H. J.; Hwang, J. Y.; Bae, D. H. Strengthening Behavior of Carbon/Metal Nanocomposites. *Sci. Rep* **2015**, *5* (1), 16114.
(17) Powell, C. J. Practical Guide for Inelastic Mean Free Paths, Effective Attenuation Lengths, Mean Escape Depths, and Information Depths in x-Ray Photoelectron Spectroscopy. *Journal of Vacuum Science & Technology A* **2020**, *38* (2), No. 023209.
(18) Giovannetti, G.; Khomyakov, P. A.; Brocks, G.; Karpan, V. M.; van den Brink, J.; Kelly, P. J. Doping Graphene with Metal Contacts. *Phys. Rev. Lett.* **2008**, *101* (2), No. 026803.
(19) Khomyakov, P. A.; Giovannetti, G.; Rusu, P. C.; Brocks, G.; van den Brink, J.; Kelly, P. J. First-Principles Study of the Interaction and Charge Transfer between Graphene and Metals. *Phys. Rev. B* **2009**, *79* (19), No. 195425.
(20) Xu, H.; Wu, X.; Li, X.; Luo, C.; Liang, F.; Orignac, E.; Zhang, J.; Chu, J. Properties of Graphene-Metal Contacts Probed by Raman Spectroscopy. *Carbon* **2018**, *127*, 491−497.
(21) Michaelson, H. B. The Work Function of the Elements and Its Periodicity. *J. Appl. Phys.* **1977**, *48* (11), 4729−4733.
(22) Levesque, P. L.; Sabri, S. S.; Aguirre, C. M.; Guillemette, J.; Siaj, M.; Desjardins, P.; Szkopek, T.; Martel, R. Probing Charge Transfer at Surfaces Using Graphene Transistors. *Nano Lett.* **2011**, *11* (1), 132−137.

(23) Park, K.; Kang, H.; Koo, S.; Lee, D.; Ryu, S. Redox-Governed Charge Doping Dictated by Interfacial Diffusion in Two-Dimensional Materials. *Nat. Commun.* **2019**, *10* (1), 4931.
(24) Yang, Y.; Brenner, K.; Murali, R. The Influence of Atmosphere on Electrical Transport in Graphene. *Carbon* **2012**, *50* (5), 1727−1733.
(25) Melios, C.; Giusca, C. E.; Panchal, V.; Kazakova, O. Water on Graphene: Review of Recent Progress. *2D Mater.* **2018**, *5* (2), No. 022001.
(26) Oh, S.-I.; Lim, J.-Y.; Kim, Y.-C.; Yoon, J.; Kim, G.-H.; Lee, J.; Sung, Y.-M.; Han, J.-H. Fabrication of Carbon Nanofiber Reinforced Aluminum Alloy Nanocomposites by a Liquid Process. *J. Alloys Compd.* **2012**, *542*, 111−117.
(27) Watanabe, E.; Conwill, A.; Tsuya, D.; Koide, Y. Low Contact Resistance Metals for Graphene Based Devices. *Diamond Relat. Mater.* **2012**, *24*, 171−174.
(28) Kim, S.; Nah, J.; Jo, I.; Shahrjerdi, D.; Colombo, L.; Yao, Z.; Tutuc, E.; Banerjee, S. K. Realization of a High Mobility Dual-Gated Graphene Field-Effect Transistor with Al2O3 Dielectric. *Appl. Phys. Lett.* **2009**, *94* (6), No. 062107.
(29) Hsu, A. L.; Koch, R. J.; Ong, M. T.; Fang, W.; Hofmann, M.; Kim, K. K.; Seyller, T.; Dresselhaus, M. S.; Reed, E. J.; Kong, J.; Palacios, T. Surface-Induced Hybridization between Graphene and Titanium. *ACS Nano* **2014**, *8* (8), 7704−7713.
(30) Freedy, K. M.; Beechem, T. E.; Litwin, P. M.; Sales, M. G.; Huang, M.; Ruoff, R. S.; McDonnell, S. J. Unraveling Chemical Interactions between Titanium and Graphene for Electrical Contact Applications. *ACS Appl. Nano Mater.* **2018**, *1* (9), 4828−4835.
(31) Fonseca, A. F.; Liang, T.; Zhang, D.; Choudhary, K.; Phillpot, S. R.; Sinnott, S. B. Graphene−Titanium Interfaces from Molecular Dynamics Simulations. *ACS Appl. Mater. Interfaces* **2017**, *9* (38), 33288−33297.
(32) Ghising, P.; Biswas, C.; Lee, Y. H. Graphene Spin Valves for Spin Logic Devices. *Adv. Mater.* **2023**, *35* (23), No. 2209137.
(33) Lu, C.-C.; Lin, Y.-C.; Yeh, C.-H.; Huang, J.-C.; Chiu, P.-W. High Mobility Flexible Graphene Field-Effect Transistors with Self-Healing Gate Dielectrics. *ACS Nano* **2012**, *6* (5), 4469−4474.
(34) Xiao, M.; Lin, Y.; Xu, L.; Deng, B.; Peng, H.; Peng, L.-M.; Zhang, Z. N-Type Dirac-Source Field-Effect Transistors Based on a Graphene/Carbon Nanotube Heterojunction. *Advanced Electronic Materials* **2020**, *6* (7), No. 2000258.

NOTE ADDED AFTER ASAP PUBLICATION

This paper was published on October 23, 2024, with an author's name misspelled. The corrected paper was reposted on October 25, 2024.

https://doi.org/10.1021/acsanm.4c04283
ACS Appl. Nano Mater. 2024, 7, 24537−24546